Opto-Electronic Science

Supplementary information

xxxx 2025, Vol. x, No. x

DOI: 10.29026/oes.2025.240029 CSTR: 32246.14.oes.2025.240029

Multi-resonance enhanced photothermal synergistic fiber-optic Tamm plasmon polariton tip for high-sensitivity and rapid hydrogen detection

Xinran Wei[1], Yuzhang Liang[1]*, Xuhui Zhang[2,3], Rui Li[1], Haonan Wei[1], Yijin He[1], Lanlan Shen[1], Yurui Fang[1], Ting Xu[4,5]* and Wei Peng[1]

[1]School of Physics, Dalian University of Technology, Dalian 116024, China; [2]Liaoning Key Laboratory of Marine Sensing and Intelligent Detection, Dalian Maritime University, Dalian 116026, China; [3]Information Science and Technology College, Dalian Maritime University, Dalian 116026, China; [4]National Laboratory of Solid-State Microstructures, College of Engineering and Applied Sciences and Collaborative Innovation Center of Advanced Microstructures, Nanjing University, Nanjing 210093, China; [5]Key Laboratory of Intelligent Optical Sensing and Manipulation, Ministry of Education, Nanjing University, Nanjing 210093, China.

*Correspondence: YZ Liang, E-mail: yzliang@dlut.edu.cn; T Xu, E-mail: xuting@nju.edu.cn

This file includes:

Supplementary information for this paper is available at https://doi.org/10.29026/oes.2025.240029

Section 1: Refractive indies of materials

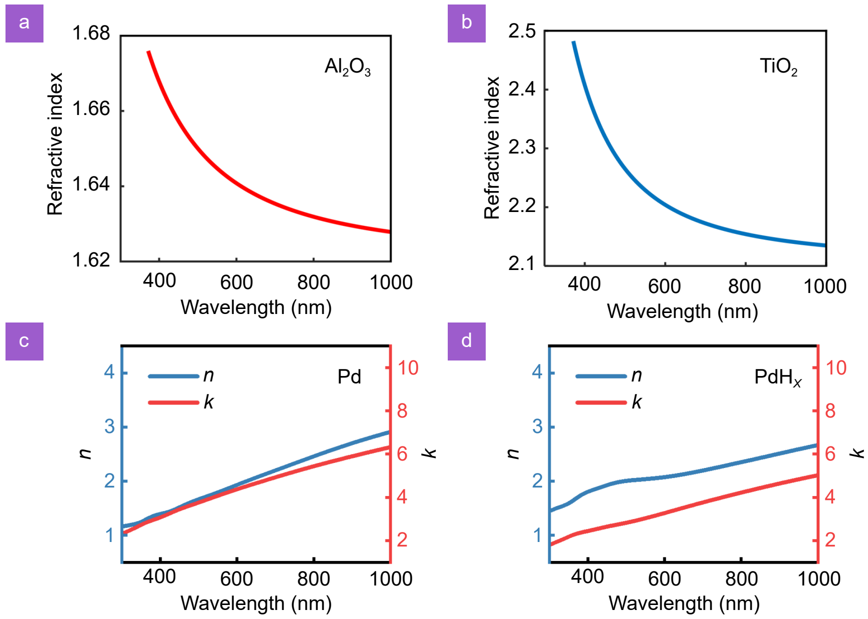

Fig. S1 | Refractive indexes of (**a**) Al_2O_3 and (**b**) TiO_2 measured by ellipsometry. Complex refractive indices of (**c**) Pd and (**d**) PdH_x reported in the literature.

Section 2: The effects of structural parameters

As shown in Fig. S2(a), with the increase of the number of bilayers of DBR, the main bandgap around 400 nm in the reflection spectrum of the FOTPP tip becomes more pronounced and stabilizes when the number of bilayers of DBR reaches 5. Additionally, the number of secondary bandgaps at longer wavelengths gradually increases. Figure S2(b) demonstrates that the deposition of the Pd film excites TPP within the main bandgap and induces FP resonance modes of various orders within the different secondary bandgaps. Besides, the quality factor of the TPP increases with the number of bilayers, but its resonance depth gradually diminishes when the number of bilayers is large. Therefore, a DBR with 5 bilayers is employed in the study. Figure S2(c, d) demonstrate that the resonance wavelengths of FOTPP tip are positively correlated with the Bragg wavelength, indicating that the operating wavelength is flexibly tunable.

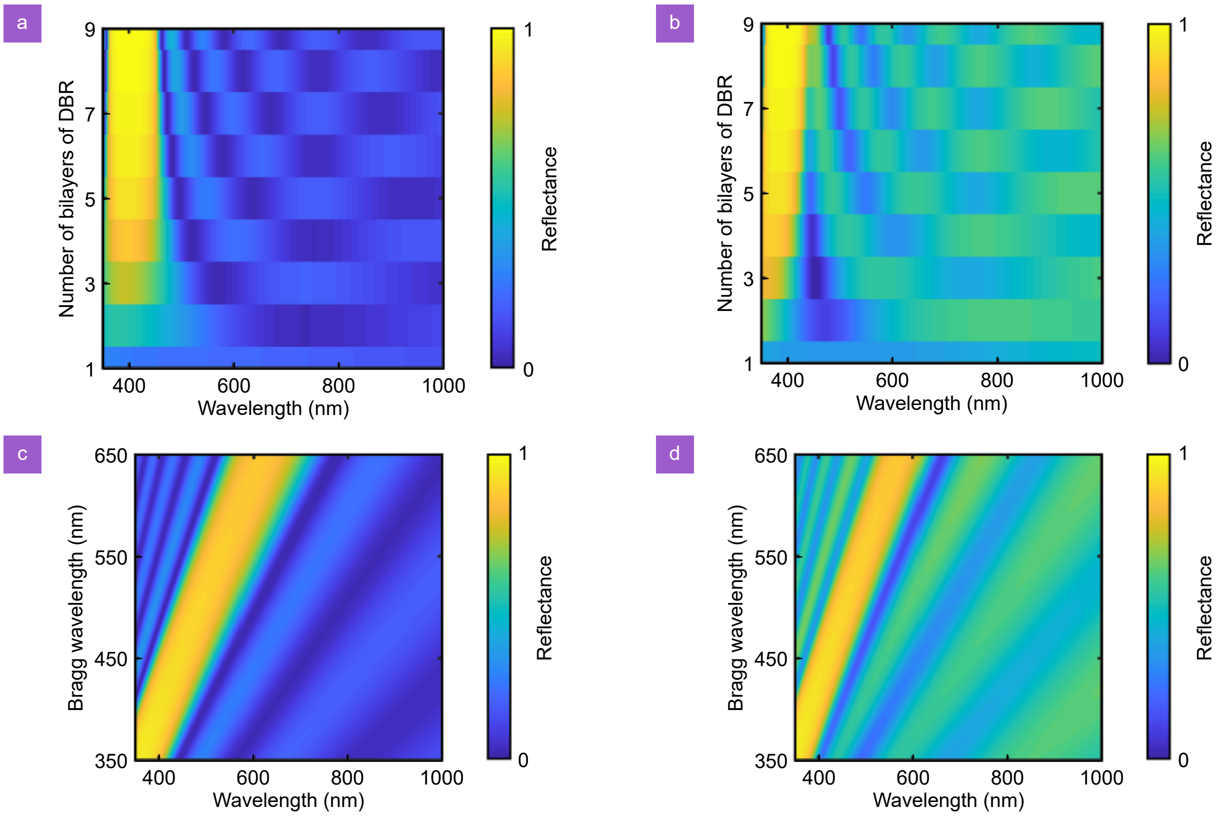

Fig. S2 | The effects of structural parameters on the characteristic spectra of the FOTPP tip. Dependence of the spectra of the FOTPP tip, both without and with a Pd film, on (**a**, **b**) the number of bilayers and (**c**, **d**) Bragg wavelength of DBR.

Section 3: Reflection phase of Pd/ PdH_x films

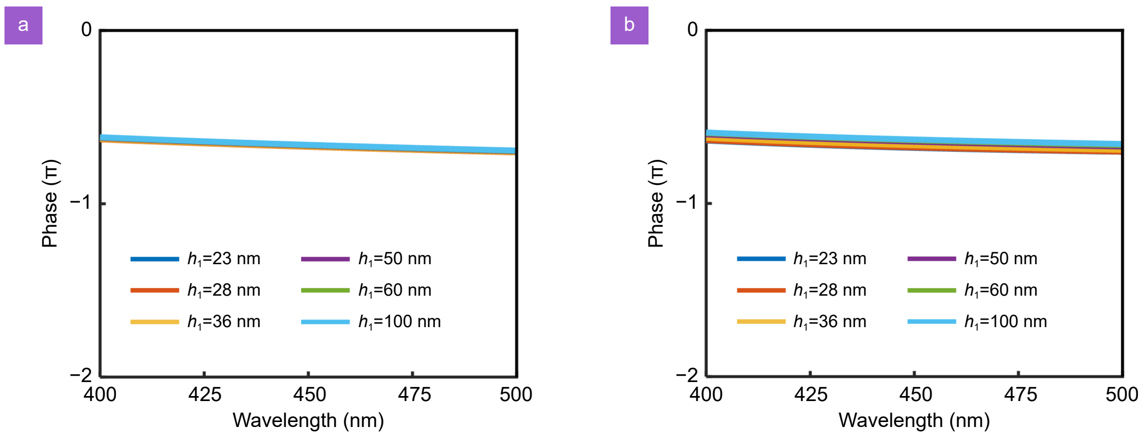

Fig. S3 | Reflection phase of (**a**) Pd and (**b**) PdH_x films at different thicknesses.

Section 4: Effect of film thickness on sensing performance

Figure S4(a, b) show the experimental spectra of the FOTPP tip with Pd films of 28 nm and 36 nm, demonstrating a red-shift with increasing H_2 concentration. For ease of comparison, their wavelength shifts are summarized in Fig. S4(c). Experimental results indicate that the FOTPP tip with the thinnest Pd film exhibits the highest sensitivity, approximately 1.24 nm/1%. The sensitivities of FOTPP tips with 36 nm and 50 nm Pd films are comparable, with the 50 nm Pd film being slightly higher, consistent with theoretical calculations. Figure S4(d, e) also show that the FOTPP tip with a thinner Pd film has a faster response and recovery speed. Therefore, to achieve greater reproducibility of the FOTPP tip's sensitivity, a thicker Pd film should be selected. In contrast, for optimal sensor performance, a thinner Pd film is preferable. Furthermore, Figure S4(f, g) demonstrate the average responses of the FOTPP tips with 28 nm and 36 nm Pd films in multiple detections of 0.5% H_2 concentration are 0.624 nm and 0.378 nm, respectively, with corresponding standard deviations of 0.0469 nm and 0.0318 nm. These small standard deviations confirm the FOTPP tips with thinner Pd films' capability for repeated detection of low-concentration H_2 and their long-term durability.

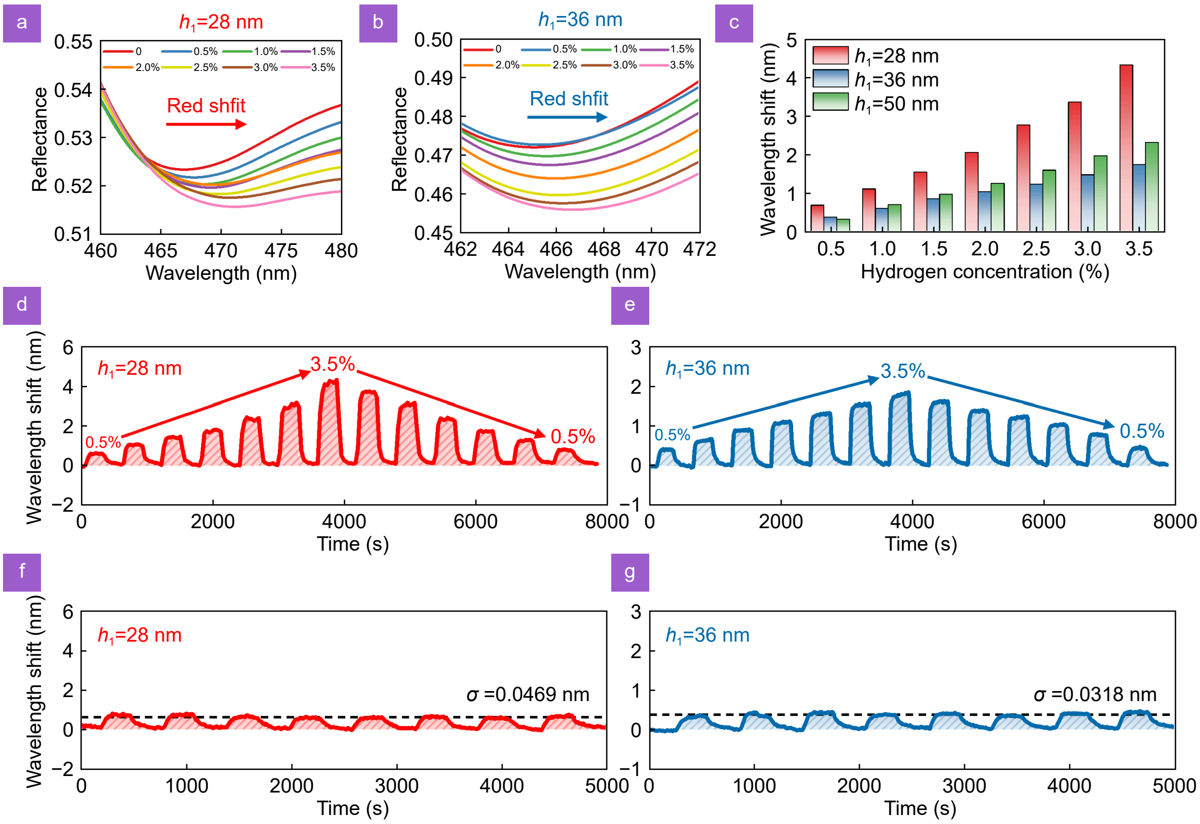

Fig. S4 | Experimental measurement of the effect of Pd film thickness on the sensing performance of FOTPP tip. Reflection spectra of the FOTPP tips with (**a**) 28 nm and (**b**) 36 nm Pd films under various H_2 concentrations ranging from 0.5% to 3.5%. (**c**) The wavelength redshifts for three distinct FOTPP tips at various H_2 concentrations. Real-time wavelength shift response of FOTPP tips with (**d**) 28 nm (**e**) 36 nm Pd films to increasing and decreasing H_2 concentration pulses, ranging from 0.5% to 3.5% and 3.5% to 0.5%. The real-time wavelength response of the FOTPP tips with (**f**) 28 nm and (**g**) 36 nm Pd films in continuously repeated 0.5% H_2 concentration detection.

Section 5: The stability of FOTPP tips

In practical applications, quantitative characterization of the stability of FOTPP, particularly under photothermal conditions, is essential. Figure S5(b–d) illustrate the resonance wavelength fluctuations of the FOTPP tips during prolonged exposure to air. The red and blue curves represent scenarios with and without photothermal assistance, respectively, with their standard deviations depicted above the curves. Experimental results show that the standard deviations of FOTPP tips are comparable under thermal and non-thermal conditions. Specifically, the maximum standard deviation is 0.0253, while the minimum standard deviation is as low as 0.0148. This underscores the excellent stability of FOTPP tips in both photothermal and non-photothermal conditions, highlighting their suitability for practical applications.

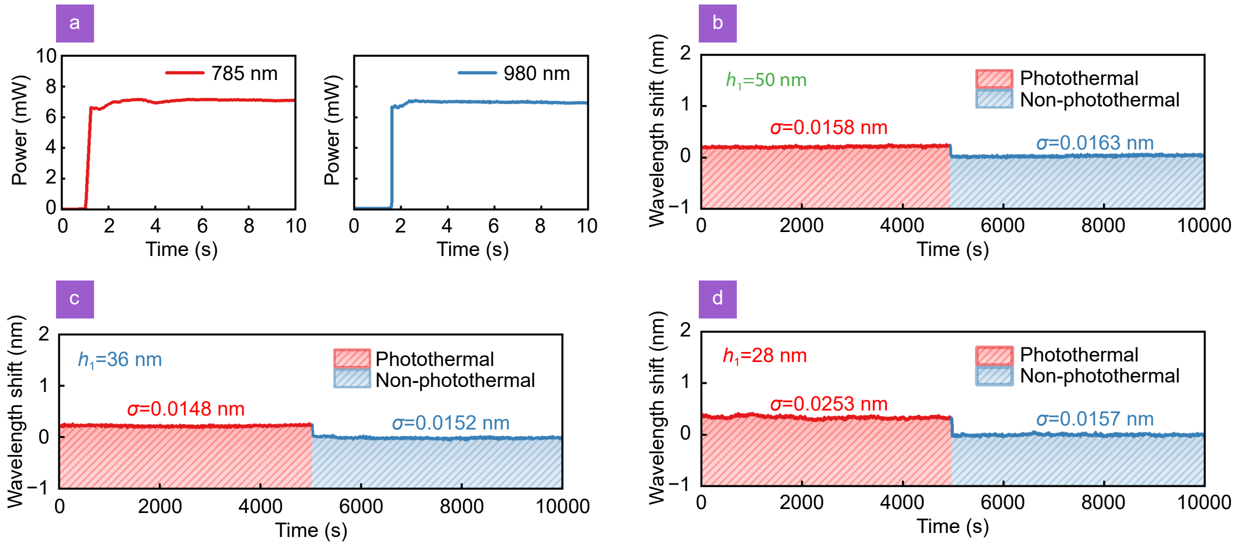

Fig. S5 | (**a**) Measured power of 785 nm and 980 nm lasers using the optical power meter. (**b**)–(**d**) Wavelength fluctuations in the air for the three different FOTPP tips, both with and without 785 nm laser photothermal conditions, where *σ* represents their respective standard deviation.

Section 6: Photothermal assistance for different Pd film thicknesses

It should be noted that the photothermal characteristics of FOTPP tips are closely related to the thickness of the Pd film. Figure S6(a) illustrates the absorption spectra around 785 nm for the three FOTPP tips with different Pd film thicknesses. The results indicate that the absorption of the FOTPP tip decreases as the Pd film thickness increases, which affects the temperature changes. Experimentally measured thermal images of the FOTPP tips with 28 nm and 36 nm Pd films are shown in Fig. S6(b) and S6(c). These images reveal that the surface temperatures of the FOTPP tips with thinner Pd films are higher, with the 28 nm Pd film showing the highest surface temperature. Figure S6(d) summarizes the surface peak temperature of the FOTPP tip from numerical simulations and experimental measurements as a function of Pd film thickness. The results further verify that the intensity of the photothermal effect is negatively correlated with the thickness of the Pd film. Furthermore, the H_2 sensing performance of FOTPP tips with 28 nm and 36 nm Pd under the photothermal assistance of a 785 nm laser has also been investigated. Figure S6(e) and S6(f) show their real-time wavelength shift responses to H_2 concentration, demonstrating that FOTPP tips with thinner Pd films also exhibit excellent response recovery characteristics and signal-to-noise ratio under photothermal assistance. Figure S6(g) and S6(h) compare the response and recovery times for FOTPP tips with three different Pd film thicknesses under photothermal assistance. All three tips exhibit response times of less than 20 s when the H_2 concentration exceeds 1.5%. The response and recovery times of the FOTPP tips correlate positively with the Pd film thickness, with the FOTPP tip featuring a 28 nm Pd film demonstrating the shortest response and recovery times of 10 s and 44 s, respectively. This is attributed to two factors: the higher permeability rate of H_2 in thinner Pd films, and the higher surface temperature of the FOTPP structure under photothermal assistance. Besides, the effect of Pd film thickness on the sensitivity of FOTPP tips under photothermal assistance is also explored. Figure S6(i) shows the wavelength redshifts of the FOTPP tips with three different Pd film thicknesses, indicating that sensitivity is negatively related to Pd film thickness, similar to the behavior without photothermal assistance. However, unlike the non-photothermal case, the sensitivity of the 50 nm Pd film is slightly lower compared to the 36 nm Pd film, which is attributed to the higher hydrogenation ratio of the 36 nm Pd film under photothermal assistance.

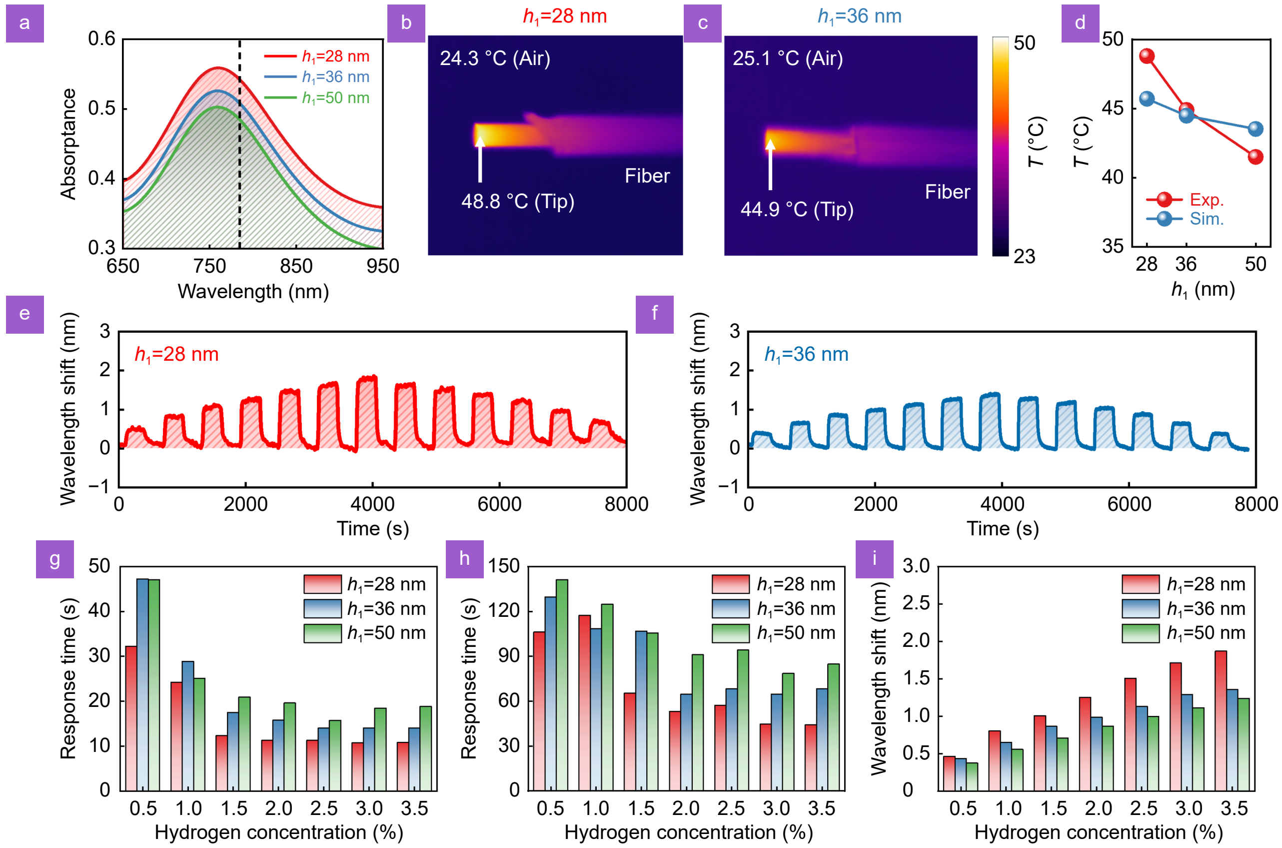

Fig. S6 | Dependence of photothermal effect and photothermal-assisted sensing performance of FOTPP tips on Pd film thickness. (**a**) Comparison of the absorption spectra near the 785 nm wavelength for the three FOTPP tips with different Pd film thicknesses. Experimentally measured thermal images of the FOTPP tips with a (**b**) 28 nm and (**c**) 36 nm Pd film. (**d**) The relationship between the surface peak temperature of the FOTPP tip with the thickness of the Pd film, as determined from numerical simulations (blue marks) and experimental measurements (red marks). Real-time wavelength shift response of the FOTPP tips with (**e**) 28 nm and (**f**) 36 nm Pd film. (**g**) Response time, (**h**) recovery time, and (**i**) wavelength redshifts for the FOTPP tips with Pd films of three different thicknesses at various H_2 concentrations.

Table S1 | Comparison of the sensing performances of fiber-optic H_2 sensors reported in recent years.

Reference	Resonance structure	Sensitivity (nm/1%)	Response time (s)	Manufacture method
ref.[S1]	Fiber grating based on doped Pt/WO_3	1.2	25 (2% H_2)	The sol-gel method + Lithography
ref.[S2]	Bragg gratings in a helical-core fiber	0.017	101 (2% H_2)	Arc discharge method + Fiber fusion + Lithography
ref.[S3]	FP structure with a deformable Pd film	0.155	100 (1% H_2)	Fiber fusion + UV curable adhesive transfer
ref.[S4]	Fiber grating based TBAOH intercalated WO_3	0.16	34 (1% H_2)	Chemical synthesis + Lithography
ref.[S5]	Optomechanical nanofilm resonator with a Pd- and graphene	Nonlinear	120.3 (0.1% H_2)	Fiber splicing + Film transfer + FIB
ref.[S6]	FP structure with Au/Pd composite film	0.153	12 (2% H_2)	Fiber fusion + UV curable adhesive transfer
ref.[S7]	FP interferometer with a fiber grating and a nanofilm	~0.064	4.3 (3.5% H_2)	Fiber fusion + Wet transfer + Lithography
This work	**TPP planar structure**	**~1.24**	**11 (2%–3.5% H_2)**	**Thin film deposition**

Note: When multiple sensing performance metrics are reported, the highest sensing performance is used for comparison.

References

S1. Wang CQ, Han ZW, Wang CX et al. Highly sensitive fiber grating hydrogen sensor based on hydrogen-doped Pt/WO_3. *Sens Actuators B Chem* **404**, 135250 (2024).

S2. Zhi YY, Hu YY, Chen H et al. Hydrogen and temperature measurement using a functionalized superstructure of Bragg gratings in a helical-

core fiber. *Opt Laser Technol* **174**, 110551 (2024).
S3. Zhang XP, Li XT, Zhang XH et al. Photothermal-assisted hydrogen permeation enhancement. *Sens Actuators B Chem* **365**, 131935 (2022).
S4. Ye Z, Ruan HB, Hu XY et al. TBAOH intercalated WO_3 for high-performance optical fiber hydrogen sensor. *Int J Hydrogen Energy* **47**, 28204–28211 (2022).
S5. Luo JX, Liu S, Chen PJ et al. Highly sensitive hydrogen sensor based on an optical driven nanofilm resonator. *ACS Appl Mater Interfaces* **14**, 29357–29365 (2022).
S6. Zhang XH, Zhang XP, Li XT et al. The nanophotonic machinal cavity and its hydrogen sensing application. *Sens Actuators B Chem* **367**, 132095 (2022).
S7. Luo JX, Liu S, Chen PJ et al. Fiber optic hydrogen sensor based on a Fabry–Perot interferometer with a fiber Bragg grating and a nanofilm. *Lab Chip* **21**, 1752–1758 (2021).